JOURNAL OF SOLID STATE CHEMISTRY 44, 415–424 (1982)

The Pressure-Induced Black Phosphorus to A7 (Arsenic) Phase Transformation: An Analysis Using the Concept of Orbital Symmetry Conservation

JEREMY K. BURDETT AND STEPHEN LEE

Department of Chemistry, The University of Chicago, Chicago, Illinois 60637

Received May 12, 1982

Orbital correlation diagrams for the black phosphorus to A7 (arsenic) phase transformation for various points in the Brillouin zone are presented and analyzed in symmetry terms. The level doublings observed at the black phosphorus geometry for several points are directly attributable to the nonsymmorphic nature of the space group (Herring's theorem). Doublings observed at the A7 structure derive from the choice of a four-atom, rather than two-atom, unit cell to view the geometrical transformation. The space group requirements at the beginning and end points of the transformation process simply control the form of orbital correlation diagrams. In general, HOMO/LUMO crossings are found at $k = (\frac{1}{2},\alpha,\beta)$ where bonds are made and broken along the x direction, a result with simple analogies to more easily visualized one-dimensional problems.

Introduction

The idea of the conservation of orbital symmetry during a concerted molecular process led, during the mid-1960s, to the Woodward–Hoffmann rules for organic reactions (*1*). With breathtaking simplicity, the question of whether chemical reactions along particular pathways were thermally allowed or forbidden could be tackled using symmetry-based ideas. Figure 1a shows an orbital energy (E) versus reaction coordinate (q) diagram for a thermally allowed process in the Woodward–Hoffmann sense. Note that the highest occupied molecular orbit (HOMO) of the reactant correlates with that of the product. In Fig. 1b we show a similar diagram for a thermally forbidden process. Note that here HOMO and LUMO (lowest unoccupied orbital) of different symmetry cross at q_c. Since the HOMO–LUMO separation in stable molecules is invariably large, such a crossing in Fig. 1b demands a high, symmetry-imposed activation energy barrier for reaction, not present in Fig. 1a.

Recently we have applied similar logic to the question of polymorphic phase transformations in solids (*2*). Here the problem is much more complex since now the $E(q)$ diagram has to be replaced by a set of $E(\mathbf{k},q)$ diagrams, where the wavevector $\mathbf{k}$ maps out the Brillouin zone of the solid. In the molecular case a single diagram carrying symmetry labels appropriate to the molecular point groups of reactant, product, and intermediate geometries was sufficient for the purpose. In the solid-state environment a set of diagrams for a representative set of $\mathbf{k}$ vectors needs to be constructed, where the symmetry labels are those appropriate to the group of the wavevector within the relevant space group. At high symmetry $\mathbf{k}$ points the group of the wavevector may

0022-4596/82/120415-10$02.00/0

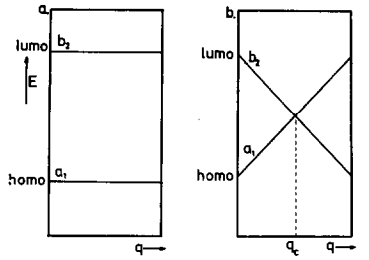

FIG. 1. (a) Noncrossing of HOMO and LUMO to give rise to a symmetry-allowed thermal process, (b) crossing of HOMO and LUMO to give rise to a symmetry-forbidden thermal process.

contain a respectably sized subgroup of the holohedral point group with several distinct representations. For **k** points which do not lie at symmetry points, or on symmetry lines or planes, then the group of the wavevector is simply C_1 and all functions will transform as the a representation. HOMO–LUMO crossings (or indeed any other orbital crossings) are then forbidden via the noncrossing rule. Only at symmetry points, therefore, may orbital crossings occur in principle to give a thermally forbidden process in a Woodward–Hoffmann sense. Away from these locations no such crossings are allowed, although it will usually be difficult to distinguish a narrowly avoided crossing at a **k** point close to a symmetry point where such a crossing does occur. The overall result is that for whole regions of the Brillouin zone, around symmetry points where a HOMO–LUMO crossing exists, there will also be high energy barriers arising from such avoided crossings. Thus, although symmetry is lost on moving away from symmetry points in the zone, much of the energetic information is "remembered" by lower symmetry points close by. In our earlier study (*2*), we presented without much comment $E(\mathbf{k},q)$ diagrams evaluated numerically using a tight-binding method at several high-symmetry points in the Brillouin zone. In this paper we examine symmetry aspects of these results.

The Black Phosphorus to A7 (Arsenic) Transformation

We recently showed (*3*, *4*) how the black phosphorus, arsenic, and other related arrangements were readily derived, both geometrically and electronically, from that of the rocksalt (or the primitive cubic) structure by the selective fission of three mutually orthogonal linkages at each atomic center. The result was the replacement of octahedral six-coordination by a universal trigonal pyramidal geometry. Some of the arsenic-like structures appear to be interconvertible under pressure. Jamieson demonstrated the pressure-induced black phosphorus to A7 transition (*5*) and three different arrangements related by temperature and pressure have been identified (*6*) for $BaSi_2$, a species isoelectronic with phosphorus itself. We shall study in this paper the former process via the geometrical transformation shown in the idealization of Fig. 2, where half of the linkages broken in the rock salt → black phosphorus, arsenic process were remade in the intermediate. Figure 3 shows a set of calculated level correlation diagrams $E(\mathbf{k},q)$ for several high-symmetry points in the Brillouin zone. Note the HOMO–LUMO crossings at $(\frac{1}{2},0,0)$ and $(\frac{1}{2},\frac{1}{2},\frac{1}{2})$ and the HOMO–LUMO touching at the A7 structure at $(\frac{1}{2},\frac{1}{2},0)$.

The unit cells used in our study are shown in Fig. 4 along with the symmetry elements present. With this choice of cell it is perhaps difficult to see the threefold rotation axis in the arsenic structure. (It appears along one of the body diagonals of the large cube in Fig. 2). There are some features of interest. The arsenic structure requires only two atoms per cell for its definition. We have twice that number since we wish to correlate the levels of this cell with those of the four-atom black phosphorus cell via the intermediate geometry. Also the space group for the black phosphorus struc-

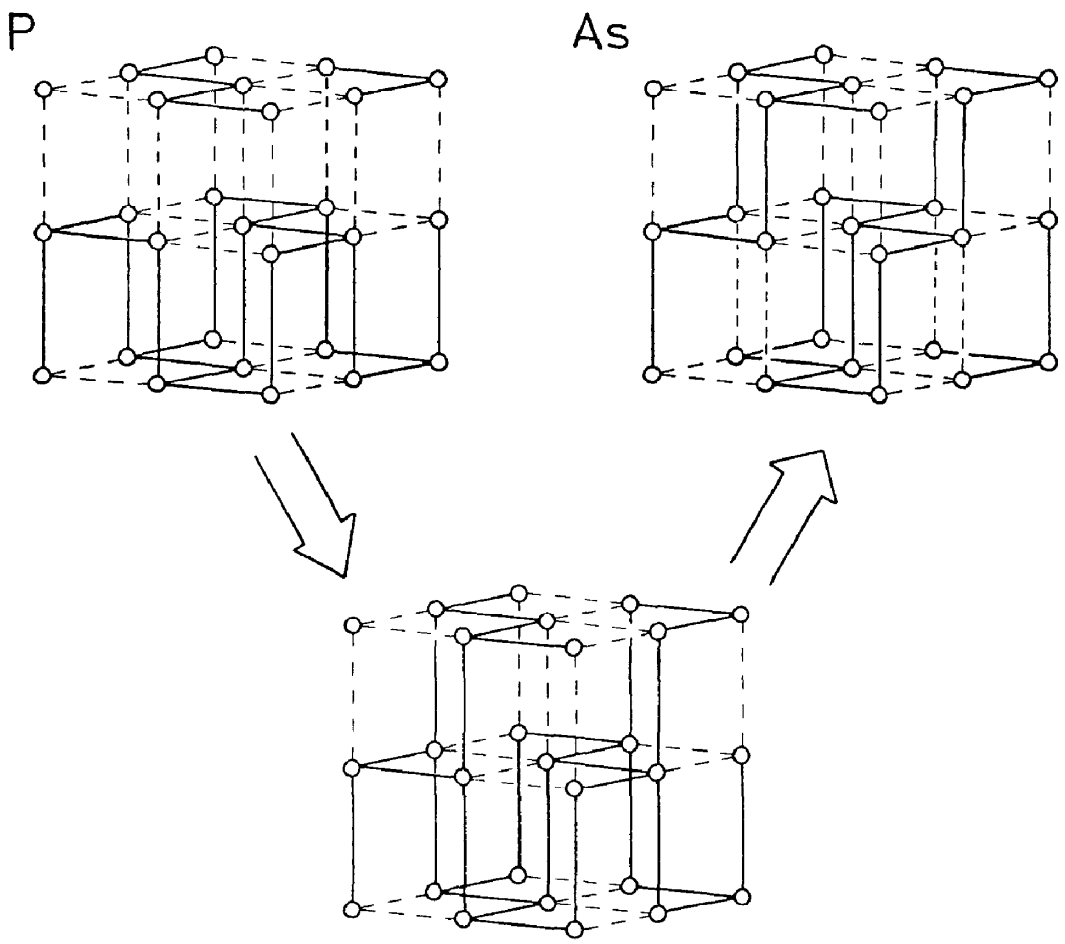

FIG. 2. One route for the interconversion of black phosphorus and arsenic. Idealization, showing relationahip to rock salt.

ture is nonsymmorphic since it contains coupled translation–rotation elements. This implies that the group of k is expanded at the zone edges and this makes derivation and handling of its representations a little more complex. Both the arsenic and intermediate space groups are symmorphic.

Symmetry Properties and Level Structure

(*a*) *The Arsenic Structure*

A feature of the level pattern at the right-hand side of each of the six panels of Fig. 3 is the presence of universal doublings at the k points $(\frac{1}{2},0,0)$, $(0,\frac{1}{2},0)$, $(0,0,\frac{1}{2})$, and $(\frac{1}{2},\frac{1}{2},\frac{1}{2})$ and occasional doublings at (0,0,0) and $(\frac{1}{2},\frac{1}{2},0)$. The former are entirely due to the use of a four-, rather than two-, atom cell, and the latter to the presence of the three-

Figure 5 shows the relationship between the four-atom cell shown in Fig. 4 and a simpler primitive two-atom cell which is just as good in defining the structure. We want to know how the levels of the two cells are related. For the four-atom cell the direct and reciprocal lattice vectors are simply

fold rotation axis, as we will now show. Such doublings are removed for $0 < q < 1$.

$$\boldsymbol{\alpha}_1 = a(2^{1/2},0,0), \quad \boldsymbol{\beta}_1 = \frac{2\pi}{a}\left(\frac{1}{2^{1/2}},0,0\right),$$

$$\boldsymbol{\alpha}_2 = a(0,1,0), \quad \boldsymbol{\beta}_2 = \frac{2\pi}{a}(0,1,0), \qquad (1)$$

$$\boldsymbol{\alpha}_3 = a(0,0,1), \quad \boldsymbol{\beta}_3 = \frac{2\pi}{a}(0,0,1).$$

For the two-atom cell the corresponding relationships are

$$\mathbf{A}_1 = a\left(-\frac{1}{2^{1/2}},\tfrac{1}{2},\tfrac{1}{2}\right), \quad \mathbf{B}_1 = \frac{2\pi}{a}(0,1,1),$$

$$\mathbf{A}_2 = a\left(\frac{1}{2^{1/2}},-\tfrac{1}{2},\tfrac{1}{2}\right), \quad \mathbf{B}_2 = \frac{2\pi}{a}\left(\frac{1}{2^{1/2}},0,1\right),$$

$$\mathbf{A}_3 = a\left(\frac{1}{2^{1/2}},\tfrac{1}{2},-\tfrac{1}{2}\right), \quad \mathbf{B}_3 = \frac{2\pi}{a}\left(\frac{1}{2^{1/2}},1,0\right). \qquad (2)$$

Clearly the phase factor on any center will be such that any property will be independent of the unit cell choice. If $\mathbf{r}$ is a member of the direct lattice then we need to seek the conditions on the k_i such that

$$(K_1\boldsymbol{\beta}_1 + K_2\boldsymbol{\beta}_2 + K_3\boldsymbol{\beta}_3)\cdot\mathbf{r} = (k_1\mathbf{B}_1 + k_2\mathbf{B}_2 + k_3\mathbf{B}_3)\cdot\mathbf{r} + 2m\pi. \qquad (3)$$

The two possible solutions are

$$\begin{aligned} k_1 &= \tfrac{1}{2}(K_2 + K_3 - K_1), & \tfrac{1}{2}(K_2 + K_3 - K_1) + \tfrac{1}{2},\\ k_2 &= \tfrac{1}{2}(K_1 + K_3 - K_2), & \tfrac{1}{2}(K_1 + K_3 - K_2) + \tfrac{1}{2},\\ k_3 &= \tfrac{1}{2}(K_1 + K_2 - K_3), & \tfrac{1}{2}(K_1 + K_2 - K_3) + \tfrac{1}{2}. \end{aligned} \qquad (4a)$$

On substitution of the values for the symmetry points used in Fig. 3, Table I is immediately generated. Note that for the points $(\frac{1}{2},0,0)_\beta$, $(0,\frac{1}{2},0)_\beta$, $(0,0,\frac{1}{2})_\beta$, and $(\frac{1}{2},\frac{1}{2},\frac{1}{2})_\beta$ the two **k** vectors generated by this decomposition belong to the same star and are therefore degenerate. So *all* the levels for the arsenic structure at these **k** points in Fig. 3 are doubled. The doublings sometimes seen at $(0,0,0)_\beta$ and $(\frac{1}{2},\frac{1}{2},0)_\beta$ are readily understood since these decompose into $(0,0,0)_B$ and $(0,0,\frac{1}{2})_B$ vectors in the two-atom unit cell. Both of these have full D_{3d} holohedral symmetry (they both lie on the threefold rotation axis) which can support doubly degenerate representations. Thus some of the levels at these points will be degenerate and others will not.

(*b*) *The Intermediate Structure*

This presents no problems at all. The symmetry operations shown in Fig. 4 lead to a symmorphic space group. The group of **k** is simply C_{2h} at all the **k** points we used in

TABLE I

RELATIONSHIP BETWEEN THE **k** POINTS IN THE FOUR-ATOM (β LABELS) AND TWO-ATOM (B LABELS) UNIT CELLS (FIG. 5) FOR THE A7 ARRANGEMENT

Four-atom cell	Two-atom cell	Label[a]	Group of **k**
$(0,0,0)_\beta$	$(0,0,0)_B$	Γ	D_{3d}
	$(\frac{1}{2},\frac{1}{2},\frac{1}{2})_B$	H	C_{2h}
$(\frac{1}{2},0,0)_\beta$	$(-\frac{1}{4},\frac{1}{4},\frac{1}{4})_B$	Degenerate	C_s
	$(\frac{1}{4},-\frac{1}{4},-\frac{1}{4})_B$		
$(0,\frac{1}{2},0)_\beta$	$(\frac{1}{4},-\frac{1}{4},\frac{1}{4})_B$	Degenerate	C_s
	$(-\frac{1}{4},\frac{1}{4},-\frac{1}{4})_B$		
$(0,0,\frac{1}{2})_\beta$	$(\frac{1}{4},\frac{1}{4},-\frac{1}{4})_B$	Degenerate	C_2
	$(-\frac{1}{4},-\frac{1}{4},\frac{1}{4})_B$		
$(\frac{1}{2},\frac{1}{2},\frac{1}{2})_\beta$	$(\frac{1}{4},\frac{1}{4},\frac{1}{4})_B$	Degenerate	C_2
	$(-\frac{1}{4},-\frac{1}{4},-\frac{1}{4})_B$		
$(\frac{1}{2},\frac{1}{2},0)_\beta$	$(0,0,\frac{1}{2})_B$	X	D_{3h}
	$(\frac{1}{2},\frac{1}{2},0)_B$	Z	C_{2h}

[a] It will be useful later on to label the energy levels of the four-atom cell using a complete notation which includes the origin of the levels in terms of the **k** points of the two-atom cell.

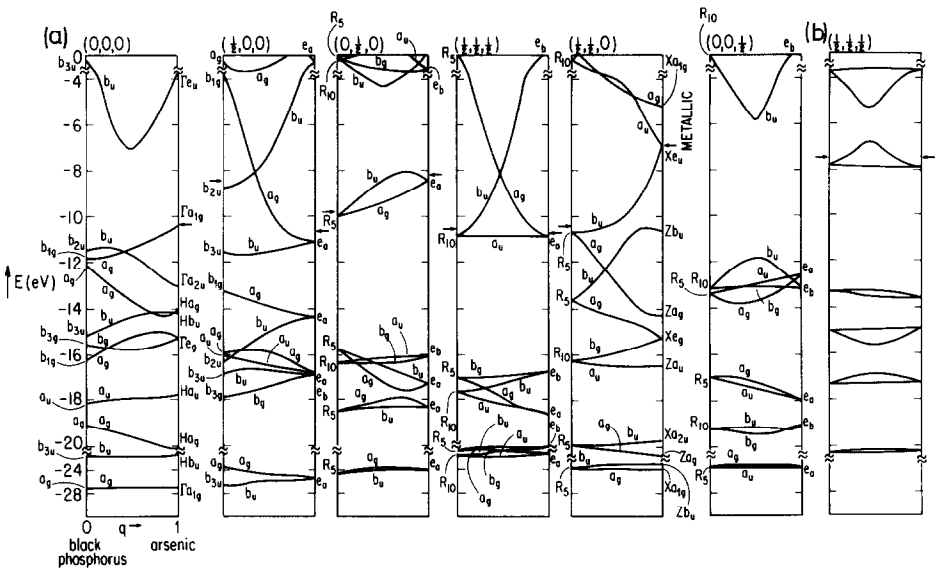

FIG. 3. Calculated $E(\mathbf{k},q)$ diagrams for the real process of Fig. 2 (adapted from Ref. (*2*)). (The symmetry labels for the intermediate levels are different from those used earlier (*2*). The difference lies in the choice of the location of the symmetry elements. In this paper the set shown in Fig. 4 has been used).

Fig. 3. None of the levels are then degenerate by reasons of symmetry (except at the special case of $q = 0.5$).

(*c*) *The Black Phosphorus Structure*

The space group of this structure is nonsymmorphic. Herring's theorem (*7*) leads to an immediate indication of the doublings of levels seen at the left-hand side of some of the panels of Fig. 3. "If a boundary plane of the Brillouin zone is perpendicular to a twofold screw axis, no element of whose coset is a pure twofold rotation, then the energy bands must stick together in pairs." In our case the screw axis is shown in Fig. 4. Thus all levels will be doubly degenerate at $(\frac{1}{2},\frac{1}{2},\frac{1}{2})$, $(0,\frac{1}{2},0)$, and $(\frac{1}{2},\frac{1}{2},0)$ as observed. The doublings at $(0,0,\frac{1}{2})$ are then due to another effect.

For points inside the Brillouin zone the space group may be treated as if it were symmorphic. Thus at (0,0,0) the group of $\mathbf{k}$ is simply D_{2h} and no doublings are seen. At $(\frac{1}{2},0,0)$ the 16-element group very simply decomposes into a direct product group $D_{2h}\otimes\{\{e|000\},\{e|100\}\}$. This means we can use the D_{2h} point group at this point too. No doubly degenerate representations are supported by this point group and indeed no doublings are observed in Fig. 3.

For the other $\mathbf{k}$ points at the boundaries of the Brillouin zone we have to employ larger groups which contain translational–rotational symmetry elements. One way to tackle this expanded problem is to use the

TABLE II

SYMMETRY ELEMENTS AND ORBITAL REPRESENTATIONS FOR THE ABSTRACT GROUP G_{16}^{9}

k point	C_1	C_2	C_3	C_4	n_5[a]	n_{10}
$0,\frac{1}{2},0$	$\{e\|000\}$	$\{e\|010\}$	$\{\sigma_x\|000\}$	$\{\sigma_x\|010\}$	6	2
$\frac{1}{2},\frac{1}{2},\frac{1}{2}$	$\{e\|000\}$	$\{e\|100\}$	$\{i\|000\}$	$\{i\|100\}$	4	4
$\frac{1}{2},\frac{1}{2},0$	$\{e\|000\}$	$\{e\|010\}$	$\{\sigma_z\|000\}$	$\{\sigma_z\|010\}$	6	2
$0,0,\frac{1}{2}$	$\{e\|000\}$	$\{e\|001\}$	$\{2_z\|000\}$	$\{2_z\|001\}$	4	4

[a] $\Gamma_{AO} = n_5R_5 + n_{10}R_{10}$ for the set of four s- and twelve p-type orbitals in the four-atom cell.

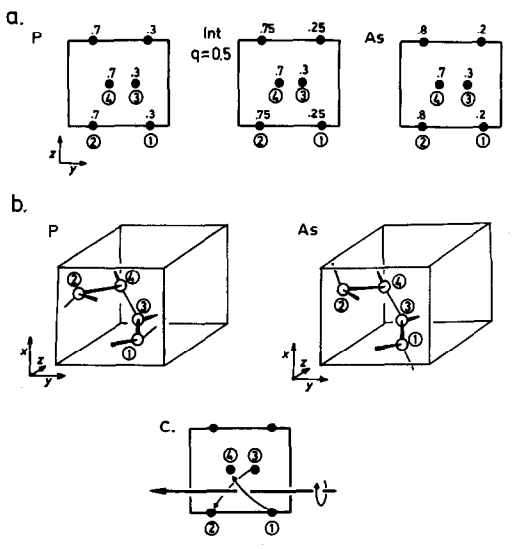

FIG. 4. (a) Unit cells for the black phosphorus, intermediate, and A7 (arsenic) structures, (b) clinographic projection of reactant and product geometries, and (c) illustration of one of the twofold screw axes in the black phosphorus structure. The symmetry elements in the three structures are as follows: (a) black phosphorus $\{e|000\}$, $\{i|000\}$, $\{2_y|0\frac{1}{2}\frac{1}{2}\}$, $\{2_x|0\frac{1}{2}\frac{1}{2}\}$, $\{\sigma_z|000\}$, $\{2_z|000\}$, $\{\sigma_x|0\frac{1}{2}\frac{1}{2}\}$, $\{\sigma_y|0\frac{1}{2}\frac{1}{2}\}$; (b) intermediate $\{e|000\}$, $\{2_z|000\}$, $\{\sigma_z|000\}$, $\{i|000\}$; (c) arsenic $\{e|000\}$, $\{i|000\}$, $\{\sigma_x|000\}$, $\{\sigma_\alpha|000\}$, $\{\sigma_\gamma|000\}$, $\{2_x|000\}$, $\{2_\alpha|000\}$, $\{2_\gamma|000\}$, $\{3_\beta^{\pm}|000\}$, $\{i6_\beta^{\pm}|000\}$ ($\alpha = 2^{1/2}x + y + z, \beta = 2^{1/2}/2x + y, \gamma = 2^{1/2}x + y - z$). Here an n-fold rotation axis (i = improper rotation) parallel to j is labeled n_j and in σ_k, k defines the direction of the plane normal.

abstract groups tabulated by Bradley and Cracknall (*8*). At the point $(0,\frac{1}{2},0)$ the group of **k** is G_{16}^9 with $C_1 = \{e|000\}$, $C_2 = \{e|010\}$, $C_3 = \{\sigma_z|000\}$, and $C_4 = \{\sigma_z|010\}$. Using the four s-type and twelve p-type atomic orbitals in the unit cell as a basis for a representation it is simple to find that $\Gamma_{AO} = 6R_5 + 2R_{10}$, where both R_5 and R_{10} are doubly degenerate representations. At $(\frac{1}{2},\frac{1}{2},\frac{1}{2})$ we can use the same abstract group but now with $C_1 = \{e|000\}$, $C_2 = \{e|100\}$, $C_3 = \{i|000\}$, and $C_4 = \{i|100\}$. At this point $\Gamma_{AO} = 4R_5 + 4R_{10}$. Analogous reasoning for the other symmetry points leads to Table II and shows that every level is doubly degenerate at these points for the black phosphorus structure. Now this result has dropped out simply from a general group theoretical approach, but Herring's theorem only demanded degeneracies for the first three points. The behavior at $(0,0,\frac{1}{2})$ is, however, readily understood. The class structure of G_{16}^9 at this **k** point is such that the two operations $\{i|000\}$ and $\{i|001\}$ compose a single class, as can be checked by running through the usual group conjugacy relationships. This requires, then, that for all symmetry species they have the same character, i.e.,

$$\chi(\{i|000\}) = \chi(\{i|001\}. \tag{4b}$$

However, we also know that

$$\{i|001\} = \{e|001\} \times \{i|000\}. \tag{5}$$

This implies that the representations are related in a similar fashion,

$$D\{i|001\} = D\{e|001\} \times D\{i|000\}. \tag{6}$$

But we can simply evaluate the representations of the regular translation $\{e|001\}$ as -1. Thus

$$\chi(\{i|000\}) = -1 \cdot \chi(\{i|001\}). \tag{7}$$

Equations (4b) and (7) together require $\chi(\{i|000\}) = 0$ for any representation and this then demands the absence of any one-dimensional representations for the group of **k** at this point.

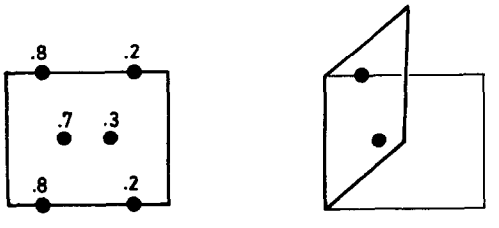

FIG. 5. The four- and two-atom arsenic unit cells.

The Form of the Wavefunctions

After having examined the broad symmetry aspects of the problem and understood the origins of the forced orbital degeneracies, it remains to see how these require-

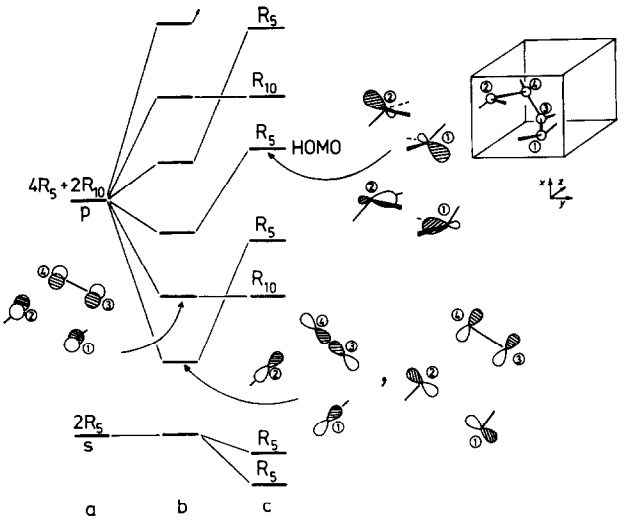

FIG. 6. Generation of the level structure for black phosphorus at $(0,\frac{1}{2},0)$. (a) Atomic orbitals, (b) simplified p-only model, and (c) complete picture with all s and p orbitals included. (b) shows the orbital character using the simplest p-only orbital model. The π- and σ-type R_5 levels actually mix together somewhat. This is shown fully in (c) for the HOMO after s-orbital interaction has been included. Because of obvious space restriction it is only possible to show limited information concerning the wavefunction. For the R_{10} level we show the composition of one component in its entirety. For the R_5 level in (b) we show both components and for the R_5 level in (c) we show that part for the wavefunction for atoms 1,2 only for both components.

ments influence the wavefunctions at various **k** and q points, and thus how the correlation diagrams of Fig. 3 arise. Since we identified the wavevector group for all the **k** points used for each geometry, it is now a relatively simple, but perhaps tedious, matter to project out suitable symmetry-adapted linear combinations of valence s and p functions located on each center. Table III shows the results which will be very useful in tracing the orbital patterns of Fig. 3. Nomenclature in this area, haphazard at best, varies from author to author. In this table we used standard labels from Ref. (*8*) when using the group G_{16}^{9} and conventional Mulliken symbols elsewhere. For some **k** points at the A7 geometry we used composite labels which describe both the level symmetry and their origin (Γ, Z, X, etc.) within the Brillouin zone of the two-atom unit cell from Table I.

First we need to know something about the orbital description of the levels of Fig. 3. Naturally this will depend crucially upon **k**. A sample analysis at one point (we choose $(0,\frac{1}{2},0)$) will illustrate a general approach which is useful. At this point the orbital transformation properties (Table III) are simple: $s \rightarrow 2R_5$, $p_z \rightarrow 2R_{10}$, and $p_x, p_y \rightarrow 4R_5$ for the black phosphorus structure. We will initially use a simple model and gradually build up in complexity. Let us neglect the s orbitals on the four atoms and focus separately on the R_{10} and R_5 manifolds of p orbitals. This leads to a very simple picture.

The pairs of p_z orbitals on atoms 1,2 and on 3,4 are coupled within purely by π interactions, and linked to each other by stronger σ interactions. (See Fig. 4 for the geometrical arrangement.) A largely bonding (between 1,2 and 3,4) pair of orbitals will result in low energy and a largely antibonding pair in higher energy (Fig. 6).

Within the R_5 manifold, if we neglect interactions between the pair of atom pairs 1,2 and 3,4 then the problem reduces to two identical 4×4 determinants containing the interactions between the p_x,p_y orbitals of each pair. This simple diatomic-like problem gives bonding and antibonding sets of orbitals of π and s type. Allowing interaction between the pairs 1,2 and 3,4 changes this description only slightly in that π- and σ-type R_5 interactions may now mix together. Inclusion of s orbitals to complete the picture results in a destabilization of all the hitherto purely p orbitals of R_5 symmetry. These orbitals, which were largely involved in π-type interactions, become largely lone pair orbitals and the σ-type interactions are now made up of s/p hybrid-type orbitals rather than pure p orbitals. The HOMO at this **k** point consists then of a large amount of lone pair character with some rather weaker bonding character between the directly linked 1,2 or 3,4 atoms. It is bonding between the pairs of atoms 1,2 and 3,4. Note how the transformation properties of the s,p_x,p_y orbitals and the properties of the wavevector group regulate the way these "molecular" orbitals on atoms 1,2 (and on 3,4) are constructed. With reference to Table III we can see how in one component of an R_5 level we find the combinations $s_1 + s_2$ and $s_3 - s_4$ and in the other $s_1 - s_2$ and $s_3 + s_4$. Exactly analogous results hold for the other points in the Brillouin zone.

We may repeat the above derivation for the arsenic structure at $(0,\frac{1}{2},0)$. The reasoning is very similar except that the role of the R_5 label is played by e_a and that of R_{10} by e_b. In general, of course, this will not be true and the orbital descriptions are sometimes very different. This procedure may be repeated at other **k** points and the orbital diagram may be assembled, just as in molecules, from a symmetry viewpoint, using well-established techniques, and a comparable level of understanding of the orbital structure will be achieved.

A final comment is in order concerning the symmetry species of the levels of the intermediate. These are also shown in Table III. Recalling that the group of the wavevector is D_{2h} for each **k** point we have used, the orbital symmetry combinations are readily generated. Just as in the arsenic and black phosphorus arrangements the contributions from atoms 1,2 (or 3,4) are linked by ± 1. We are now in a position to understand the correlation diagrams of Fig. 3.

The Correlation Diagrams

At the point $(0,\frac{1}{2},0)$ which we examined in detail above, Table III indicates that each R_5 or e_a representation splits into $a_g + b_u$ on moving to the intermediate structure. Analogously, $R_{10}(e_b) \rightarrow b_g + a_u$. Thus the very

TABLE III

SYMMETRY PROPERTIES OF THE ORBITALS

(a) Black phosphorus structure

(0,0,0)

a_g: $s_1 + s_2 + s_3 + s_4, x_1 - x_2 - x_4 + x_3, y_1 - y_2 + y_4 - y_3$
b_{1g}: $s_1 + s_2 - s_3 - s_4, x_1 - x_2 + x_4 - x_3, y_1 - y_2 - y_4 + y_3$
b_{2u}: $s_1 - s_2 + s_4 - s_3, x_1 + x_2 - x_4 + x_3, y_1 + y_2 + y_4 + y_3$
b_{3u}: $s_1 - s_2 - s_4 + s_3, x_1 + x_2 + x_3 + x_4, y_1 + y_2 - y_4 - y_3$
b_{2g}: $z_1 - z_2 - z_4 + z_3$
b_{3g}: $z_1 - z_2 + z_4 - z_3$
a_u: $z_1 + z_2 - z_4 - z_3$
b_{1u}: $z_1 + z_2 + z_3 + z_4$

$(\frac{1}{2},0,0)$

a_g: $s_1 - s_2 - s_4 + s_3, x_1 + x_2 + x_4 + x_3, y_1 + y_2 - y_4 - y_3$
b_{1g}: $s_1 - s_2 + s_4 - s_3, x_1 + x_2 - x_4 - x_3, y_1 + y_2 + y_4 + y_3$
b_{3u}: $s_1 + s_2 - s_4 - s_3, x_1 - x_2 + x_4 - x_3, y_1 - y_2 - y_4 + y_3$
b_{2u}: $s_1 + s_2 + s_3 + s_4, x_1 - x_2 - x_4 + x_3, y_1 - y_2 + y_4 - y_3$
b_{2g}: $z_1 + z_2 + z_4 + z_3$
b_{3g}: $z_1 + z_2 - z_4 - z_3$
a_u: $z_1 - z_2 + z_4 - z_3$
b_{1u}: $z_1 - z_2 - z_4 + z_3$

$(0,\frac{1}{2},0)$

R_5: $\{s_1 + s_2, s_3 - s_4\}, \{s_1 - s_2, s_3 + s_4\}$
$\{x_1 + x_2, x_3 - x_4\}, \{x_1 - x_2, x_3 - x_4\}$
$\{y_1 + y_2, y_3 - y_4\}, \{y_1 - y_2, y_3 + y_4\}$
R_{10}: $\{z_1 + z_2, z_3 - z_4\}, \{z_1 - z_2, z_3 + z_4\}$

$(\frac{1}{2},\frac{1}{2},\frac{1}{2})$

R_5: $\{s_1 + s_2, s_3 - s_4\}, \{x_1 - x_2, x_3 + x_4\}, \{z_1 - z_2, z_3 + z_4\}$
$\{y_1 - y_2, y_3 + y_4\}$

TABLE III—*Continued*

R_{10}: $\{s_1 - s_2, s_3 + s_4\}, \{x_1 + x_2, x_3 - x_4\}, \{z_1 + z_2, z_3 - z_4\}$
$\{y_1 + y_2, y_3 - y_4\}$

$(\frac{1}{2},\frac{1}{2},0)$

R_5: $\{s_1 + s_2, s_3 - s_4\}, \{s_1 - s_2, s_3 + s_4\}$
$\{x_1 + x_2, x_3 - x_4\}, \{x_1 - x_2, x_3 + x_4\}$
$\{y_1 + y_2, y_3 - y_4\}, \{y_1 - y_2, y_3 + y_4\}$
R_{10}: $\{z_1 + z_2, z_3 - z_4\}, \{z_1 - z_2, z_3 + z_4\}$

$(0,0,\frac{1}{2})$

R_5: $\{s_1 + s_2, s_3 + s_4\}, \{x_1 - x_2, x_3 - x_4\}, \{z_1 + z_2, z_3 + z_4\}$
$\{y_1 - y_2, y_3 - y_4\}$
R_{10}: $\{s_1 - s_2, s_3 - s_4\}, \{x_1 + x_2, x_3 + x_4\}, \{z_1 - z_2, z_3 - z_4\}$
$\{y_1 + y_2, y_3 + y_4\}$

(b) A7 structure

(0,0,0)

Γa_{1g}: $\beta_1 - \beta_2 + \beta_4 - \beta_3, s_1 + s_2 + s_3 + s_4$
Γa_{2u}: $\beta_1 + \beta_2 + \beta_4 + \beta_3, s_1 - s_2 + s_3 - s_4$
Γe_g: $\{z_1 - z_2 + z_4 - z_3, \alpha_1 - \alpha_2 + \alpha_4 - \alpha_3\}$
Γe_u: $\{z_1 + z_2 + z_4 + z_3, \alpha_1 + \alpha_2 + \alpha_4 + \alpha_3\}$
where $\alpha = (2^{1/2}/2x - y)$, $\beta = (2^{1/2}/2x - y)$
Ha_g: $s_1 + s_2 - s_3 - s_4, x_1 - x_2 - x_4 + x_3, y_1 - y_2 - y_4 + y_3$
Hb_u: $s_1 - s_2 - s_4 + s_3, x_1 + x_2 - x_4 - x_3, y_1 + y_2 - y_4 - y_3$
Hb_g: $z_1 - z_2 - z_4 + z_3$
Ha_u: $z_1 + z_2 - z_4 - z_3$

$(\frac{1}{2},0,0)$

e_a: $\{s_1 + s_2, s_3 - s_4\}, \{x_1 + x_2, x_3 - x_4\}$
$\{y_1 + y_2, y_3 - y_4\}$
$\{s_1 - s_2, s_3 + s_4\}, \{x_1 - x_2, x_3 + x_4\}$
$\{y_1 - y_2, y_3 + y_4\}$
e_b: $\{z_1 + z_2, z_3 - z_4\}$
$\{z_1 - z_2, z_3 + z_4\}$

$(0,\frac{1}{2},0)$

e_a: $\{s_1 + s_2, s_3 - s_4\}, \{x_1 + x_2, x_3 - x_4\}$
$\{y_1 + y_2, y_3 - y_4\}, \{s_1 - s_2, s_3 + s_4\}$
$\{x_1 - x_2, x_3 + x_4\}, \{y_1 - y_2, y_3 + y_4\}$
e_b: $\{z_1 + z_2, z_3 - z_4\}$
$\{z_1 - z_2, z_3 + z_4\}$

$(\frac{1}{2},\frac{1}{2},\frac{1}{2})$

e_a: $\{s_1 + s_2, s_3 + s_4\}, \{x_1 - x_2, x_3 - x_4\}, \{y_1 - y_2, y_3 - y_4\}$
$\{z_1 + z_2, z_3 + z_4\}$
e_b: $\{s_1 - s_2, s_3 - s_4\}, \{x_1 + x_2, x_3 + x_4\}, \{y_1 + y_2, y_3 + y_4\}$
$\{z_1 - z_2, z_3 - z_4\}$

$(\frac{1}{2},\frac{1}{2},0)$

Xa_{2u}: $s_1 - s_2 + s_4 - s_3, \gamma_1 + \gamma_2 + \gamma_3 + \gamma_4$
Xa_{1g}: $s_1 + s_2 + s_3 + s_4, \gamma_1 - \gamma_2 + \gamma_4 - \gamma_3$
Xe_u: $\{z_1 + z_2 + z_3 + z_4, \alpha_1 + \alpha_2 + \alpha_3 + \alpha_4\}$
Xe_g: $\{z_1 - z_2 + z_4 - z_3, \alpha_1 - \alpha_2 + \alpha_4 - \alpha_3\}$
Za_g: $s_1 + s_2 - s_3 - s_4, x_1 - x_2 - x_4 + x_3, y_1 - y_2 - y_4 + y_3$
Zb_u: $s_1 - s_2 - s_4 + s_3, x_2 - x_4 - x_3, y_1 + y_2 - y_4 - y_3$
Zb_g: $z_1 - z_2 - z_4 + z_3$
Za_u: $z_1 + z_2 - z_3 - z_4$
where $\gamma = (2^{1/2}/2x + y)$
and $\alpha = (2^{1/2}/2x - y)$

$(0,0,\frac{1}{2})$

e_a: $\{s_1 + s_2, s_3 + s_4\}, \{z_1 + z_2, z_3 + z_4\}, \{x_1 - x_2, x_3 - x_4\}$
$\{y_1 - y_2, y_3 - y_4\}$

TABLE III—*Continued*

e_b: $\{z_1 - z_2, z_3 - z_4\}, \{s_1 - s_2, s_3 - s_4\}$
$\{x_1 + x_2, x_3 + x_4\}, \{y_1 + y_2, y_3 + y_4\}$

(c) Intermediate structure

(0,0,0)

a_g: $s_1 + s_2, s_3 + s_4, x_1 - x_2, y_1 - y_2, x_3 - x_4, y_3 - y_4$
b_u: $s_1 - s_2, s_3 - s_4, x_1 + x_2, y_1 + y_2, x_3 + x_4, y_3 + y_4$
b_g: $z_1 - z_2, z_3 - z_4$
a_u: $z_1 + z_2, z_3 + z_4$

$(\frac{1}{2},0,0)$

a_g: $s_1 - s_2, s_3 - s_4, x_1 + x_2, y_1 + y_2, x_3 + x_4, y_3 + y_4$
b_u: $s_1 + s_2, s_3 + s_4, x_1 - x_2, y_1 - y_2, x_3 - x_4, y_3 - y_4$
b_g: $z_1 + z_2, z_3 + z_4$
a_u: $z_1 - z_2, z_3 - z_4$

$(0,\frac{1}{2},0)$

same as at $(\frac{1}{2},0,0)$

$(\frac{1}{2},\frac{1}{2},\frac{1}{2})$

a_g: $s_1 + s_2, x_1 - x_2, y_1 - y_2, z_3 + z_4$
b_g: $s_3 - s_4, x_3 + x_4, y_3 + y_4, z_1 - z_2$
a_u: $s_3 + s_4, x_3 - x_4, y_3 - y_4, z_1 + z_2$
b_u: $s_1 - s_2, x_1 + x_2, y_1 + y_2, z_3 - z_4$

$(\frac{1}{2},\frac{1}{2},0)$

same as at (0,0,0)

$(0,0,\frac{1}{2})$

same as at $(\frac{1}{2},\frac{1}{2},\frac{1}{2})$

A note concerning symmetry labels. R_5, R_{10} labels are those used in Ref. (*8*) for the group G_{16}^9. Labels for the A7 levels will sometimes include a reference to the **k** point of the two-atom cell (via Γ, H, X, Z) as noted in Table I combined with a standard Mulliken label. At the **k** points for the A7 structure, where all levels are doubled, the pseudolabels e_a, e_b are used, which distinguish the parity with respect to 2_z or σ_z.

simple correlation diagram shown in Fig. 3 follows for this **k** point. A similar diagram holds for the point $(0,0,\frac{1}{2})$. At these two **k** points the levels very simply correlate in pairs depending on their R_5 or R_{10} origin as dictated by the symmetry requirements of Table III. At $(\frac{1}{2},\frac{1}{2},\frac{1}{2})$, however, the situation is different. Here pairs of R_5,R_{10} levels correlate with pairs of arsenic levels and a crossing is forced between each pair of R_5,R_{10} levels. A similar crossing is seen at $(\frac{1}{2},0,0)$, where the levels originating from b_{3u} and b_{2u} at the black phosphorus structure repel each other in the intermediate as do the levels originating from b_{1g} and a_g lev-

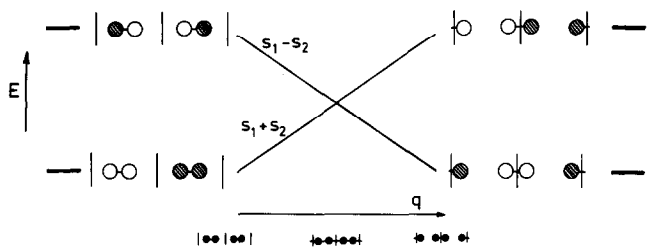

FIG. 7. HOMO–LUMO crossing for bond reorganization in the linear chain of diatomics.

els. A striking feature, therefore, at these two points, which both contain $k_x = \frac{1}{2}$, is the correlation of lone pair and antibonding orbitals along the reaction pathway. This is a result analogous to a similar crossing involved in the hypothetical bond reorganization process (in the x direction) of the linear chain of diatomic molecules at $k_x = \frac{1}{2}$ (Fig. 7). The structural instability at the halfway point, where there are equal atomic separations in the chain, is simply due to a Peierls type of distortion associated with the half-filled band. In the present case, we could imagine an identical situation for the primitive cubic structure for phosphorus (actually identified at high pressures (*5*)). Here each of three perpendicular p orbitals is half-full and the distortion to either the black phosphorus or arsenic structures of Fig. 2 is then a natural way to relieve this Fermi surface instability in each direction. Remaking the broken linkages in one Cartesian direction to get to the intermediate of Fig. 2 thus restores the instability along this direction and gives rise to a crossing of the type seen in Fig. 7.

We show how the use of symmetry arguments can be used to understand the numerical results generated by a tight-binding calculation. Much of the interest in this pedagogic exercise arises from the nature of the space groups and unit cell size of the three structures considered. The example we chose, however, does not have the simple sort of level structure typical of small organic molecules, and thus the correlation diagrams are only understandable after a considerable amount of analysis.

Acknowledgments

This research was supportd by the National Science Foundation under NSF DMR 8019741, and by the NSF–MRL program at the University of Chicago, DMR 7924007.

References

1. R. B. WOODWARD AND R. HOFFMAN, "The Conservation of Orbital Symmetry," Verlag Chemie, Weinheim (1970).
2. J. K. BURDETT AND S. L. PRICE, *Phys. Rev. B* **25**, 5778 (1982).
3. J. K. BURDETT AND T. J. MCLARNAN, *J. Chem. Phys.* **75**, 5764 (1981).
4. J. K. BURDETT, P. HAALAND, AND T. J. MCLARNAN, *J. Chem. Phys.* **75**, 5774 (1981).
5. J. C. JAMIESON, *Science* **139**, 1291 (1963).
6. J. EVERS, G. OEHLINGER, AND A. WEISS, *Z. Naturforsch. B* **32**, 1352 (1977); **34**, 358, 524 (1979); **35**, 397 (1980).
7. C. HERRING, *Phys. Rev.* **52**, 361, 365 (1937).
8. C. J. BRADLEY AND A. P. CRACKNALL, "The Mathematical Theory of Symmetry in Solids," Oxford Univ. Press, London/New York (1972).